Available online at www.sciencedirect.com
SCIENCE DIRECT®
PERGAMON
International Journal of Heat and Mass Transfer 46 (2003) 2239–2251
International Journal of HEAT and MASS TRANSFER
www.elsevier.com/locate/ijhmt

Simultaneous visualization of dry spots and bubbles for pool boiling of R-113 on a horizontal heater

Heung June Chung *, Hee Cheon No

Department of Nuclear Engineering, Korea Advanced Institute of Science and Technology, 373-1 Kusong-dong Yusong-gu, Daejon 305-701, Republic of Korea

Received 29 March 2002; received in revised form 18 September 2002

Abstract

A new experimental attempt was made to simultaneously observe the dynamic behaviors of bubbles and dry spots in the vicinity of boiling surface. Also, the two-dimensional bubble structures were obtained separately. From the visualization results, the formation of bubbles and dry spots occurs simultaneously. At critical heat flux (CHF), the surface rewetting is repeated by the local nucleate boiling around the large vapor film. At just after CHF, nucleate boiling at the locally wetted region is extinguished, resulting in the dryout of the whole heater surface. Therefore, we conclude that CHF is initiated from the locally limited nucleate boiling activity rather than any hydrodynamic instability.

Keywords: Dry spot; Bubble; Locally limited nucleate boiling activity

1. Introduction

In spite of extensive experimental and theoretical efforts there are still considerable disagreements regarding boiling characteristics and the CHF triggering mechanism. These disagreements come mainly from the lack of detailed knowledge of the physical phenomena causing the CHF on the near-wall region. As a result, almost all CHF models developed so far have described the CHF based on postulated mechanisms, which were not verified through direct observation. Therefore, in order to describe the CHF triggering mechanism accurately, direct observation of the near-wall region during boiling crisis is very important.

As a classical visual study, Gaertner [1] directly observed the boiling phenomena in the near-wall region. He hypothesized the second transition region, where the stems of the vapor mushrooms collapse causing local vapor patches to form on the heat transfer surface. He concluded that widespread vapor patches caused CHF or burnout. Based on Gaertner's experimental observation, Haramura and Katto [2] proposed the 'macrolayer dryout model' and Dhir and Liaw [3] proposed the 'unified model' for CHF.

Dry spots or dry areas on the heating surface have been reported in a number of experimental results. The occurrence of dry areas means that the heating surface is partly in contact with the liquid. The effect of dry areas on the heating surface is very important, because the dry areas have much poorer heat transfer rate than the surface covered with the liquid. Kirby and Westwater [4] investigated the liquid–vapor interactions very close to the heated surface. From their results, an important consequence is that sizable dry spots may develop under the large vapor masses, whereas only small dry spots (if any) can develop under bubbles which are small compared to the vapor mass. They concluded that the rapid growth of dry areas seems to be a prelude to the maximum heat flux. Van Ouwerkerk [5] experimentally investigated the occurrence of dry area using Pyrex or fused quartz with a conductive layer of gold having a thickness of 10 nm. When the heat flux is sufficiently

* Corresponding author. Tel.: +82-42-868-2077; fax: +82-42-868-8362.
E-mail address: hjchung@kaeri.re.kr (H.J. Chung).

0017-9310/03/$ - see front matter
doi:10.1016/S0017-9310(02)00524-0

Nomenclature

CHF(+)	just after critical heat flux
N	active nucleation site density, sites/m^2
q	heat flux, kW/m^2
q_{CHF}	critical heat flux, kW/m^2
T_{sat}	saturation temperature, K
ΔT_{ws}	surface superheat temperature, K

Greek symbols

Γ_W	wetted fraction
ρ_f	density of liquid, kg/m^3
ρ_g	density of vapor, kg/m^3

high, suddenly at some point on the heating surface a dry area is not wetted and starts growing, leading to burnout. Carvalho and Bergles [6] identified pool nucleate boiling subregimes together with the description of dry spot formation. They concluded that if the slope of the boiling curve was invariant, no dry spots were formed on the surface. And they believed, as proposed by Gaertner [1], that the primary event for the onset of CHF was the propagation of dry patches or local areas of film boiling under vapor clots to envelop the whole surface. Nishio et al. [7] observed the dynamic behavior of dry area for the pool boiling of R-113 on a sapphire plate. They pointed out that the liquid–solid contact of the network pattern at CHF is much different from the observation of Gaertner [1], and the boiling structure model by Dhir and Liaw [3] and Haramura and Katto [2], in which isolated tiny vapor stems are attached to the boiling surface.

Even though the dry spots were experimentally observed by a number of investigators as discussed above, they were not actively considered in CHF modeling so far. Very recently, Ha and No [8–10] successfully applied the behavior of dry spots to the development of CHF models.

It is evident from the above reviews that the bubble behaviors in each boiling subregime are closely related to the formation of dry areas, and these dry areas, at least, are responsible for the onset of CHF. Therefore, to obtain clear information for the CHF triggering mechanism, the synchronized observation for the behaviors of bubbles and dry areas rather than the individual observation in the vicinity of a boiling surface is essential. In the present study new experimental attempts are made to directly observe the physical boiling phenomena of bubbles and dry areas simultaneously from below the heater surface. In addition, we take side views of bubbles to obtain the two-dimensional bubble behavior.

2. Experimental method

In the present study, two cases of direct observations for the boiling surface have been carried out. First, the synchronized dynamic behaviors of bubbles and dry areas (Experiment 1) were observed by using experimental facility 1. And experimental facility 2 was used to observe the lateral bubble structures (Experiment 2). In order to maintain the consistency between two experiments, all experimental conditions are kept the same.

2.1. Description of experiment 1 for synchronized observation of dynamic behaviors of bubbles and dry areas

The experimental facility 1 was made for both pool and flow boiling tests. A schematic flow diagram of the experimental facility 1 is shown in Fig. 1. It consists of a test section, condenser, storage tank, canned motor pump, and preheater.

As shown in Fig. 2, the horizontal test section is made of 80×80 mm inner dimension mica plates that are 10 mm thick and 0.5 m long. A 10 mm thick and 50×50 mm^2 single crystal sapphire plate is installed on the central part of the bottom plate of the test section. The base surface of the sapphire plate is coated with a transparent electro-conductive (ITO: indium oxide with a trace of tin oxide) film of 700 Å. The bottom face of the heater, single crystal sapphire, is enclosed with the silicone oil bath to reduce the heat loss and to match the refractive index.

For the pool boiling test, two isolation valves at upstream and downstream of the test section are closed, and four auxiliary heaters, each of which has a maximum heat capacity of 450 W, maintains the liquid temperature as a saturation condition under atmospheric pressure.

A 250 V, 8 A DC generator, supplies electric power to the electro-conductive film, then the test liquid is boiled on the upper surface of the sapphire plate. Six K-type thermocouples, four on the lower side and two on the upper side of the sapphire plate, measure both side heater surface temperatures.

In this study an Ar-ion laser is used as a light source. As shown in Fig. 2, the laser beam reflected from the mirror is introduced to the bottom of the sapphire plate. If this incident beam is adequately set, the total reflection will occur on the upper surface of the sapphire plate when the upper heated surface is dry, while it does not

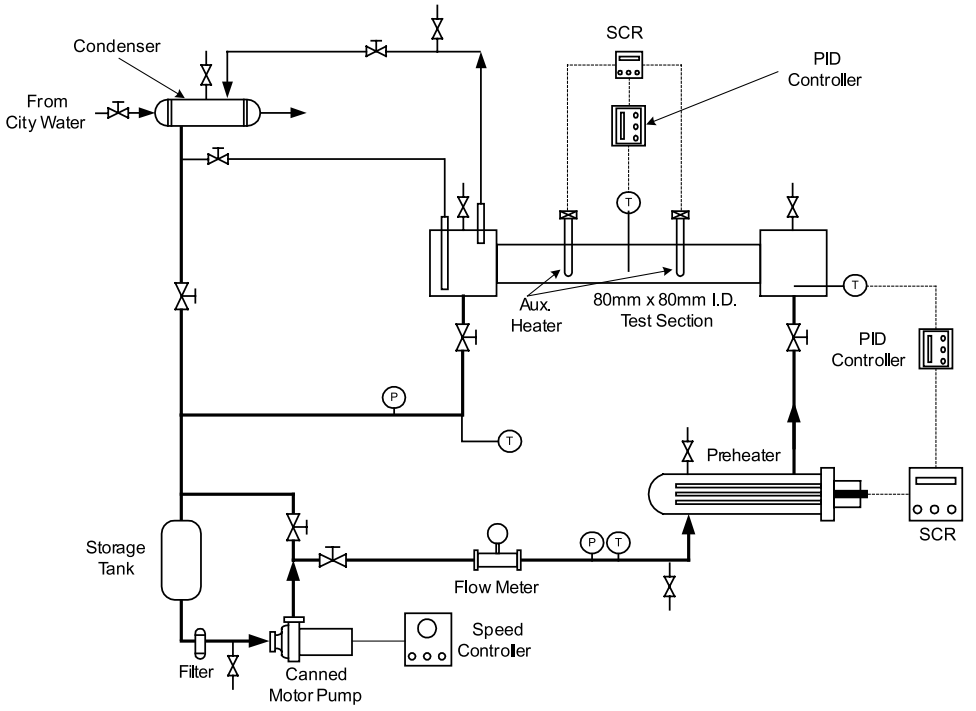

Fig. 1. Schematic flow diagram of the boiling test facility.

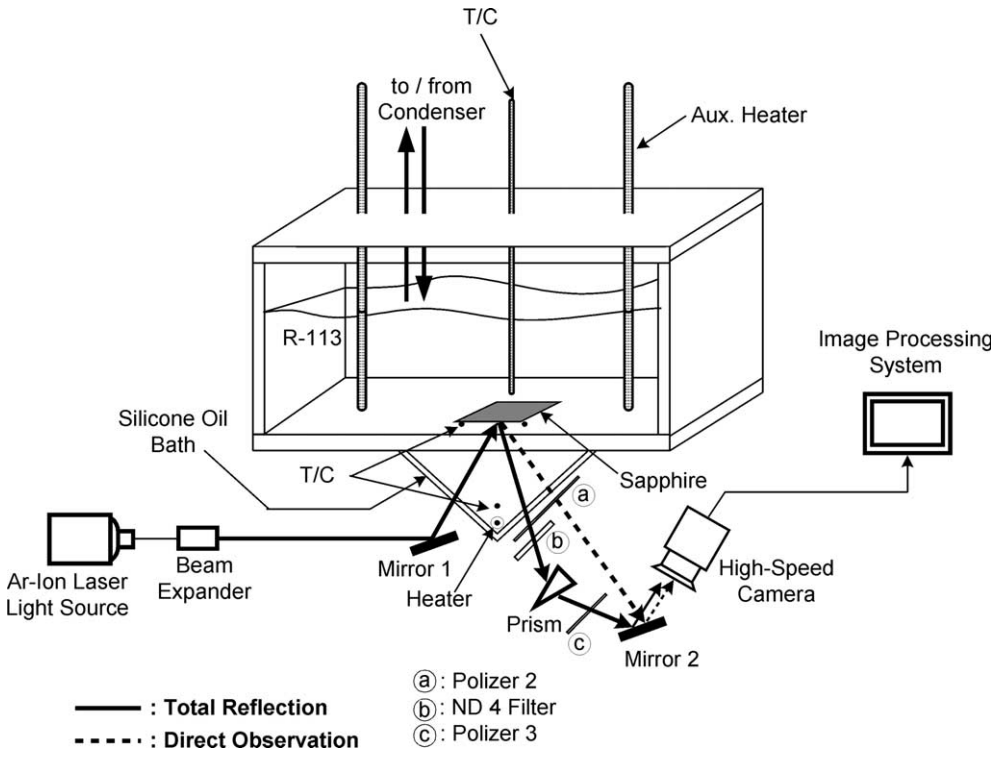

Fig. 2. Configuration of the test section with optical setup for pool boiling test.

occur when the surface is wet by the liquid. At the same time, we directly observe the bubbles on the upper heater surface.

To obtain the synchronized images of the dynamic behaviors of bubbles and dry areas, some combination of lenses and filters are arranged as shown in Fig. 2. A beam expander enlarges the incident beam from mirror 1 as it covers the whole heater surface. In order to control the total reflection beam intensity and to get clear bubble images, a polarizer 2 and a neutral density filter upstream of the prism are used. A prism with angle of 5° changes the total reflection beam path not to overlap with the direct observation beam. The polarizer 3 removes the interference fringes from the laser beam and other optical noises. Finally, mirror 2 collects the total reflection beam and direct observation beam, and then it transmits the mirror images, dry areas and bubbles, to the camera image plane.

In this study R-113 was selected as a test liquid due to its low boiling point (47.6 °C at 0.1 MPa). The boiling experiment has been carried out under the steady state condition at atmospheric pressure by adjusting the DC current step by step. And the experimental ranges covered from low to high heat flux region (CHF). The uncertainties of the heater surface temperature and heat flux were estimated from the sensors calibration and the accuracy of the equipment according to the error propagation method [21]. The evaluated maximum uncertainty of the heater surface temperature was less than ± 0.7 K. And, the uncertainty of the heat flux calculated from the applied power was always less than $\pm 1.0\%$ of the readings. For each step, motion pictures were taken by a high-speed video system which was operated at 500 frames per second.

2.2. Description of experiment 2 for observation of lateral bubble structures

To observe the bubble behavior from the lateral view, an experimental facility 2 is built up as illustrated in Fig. 3. As shown in Fig. 3(a), the test block is located in a rectangular glass vessel with inside dimensions of $150 \times 150 \times 200$ mm. A test block, Fig. 3(b), is composed of a sapphire plate, a Teflon pad and a BK-7 glass plate. The boiling surface is basically the same as that of experiment 1. A 5 mm thick and 40×5 mm single crystal sapphire plate, of which bottom face is coated with an ITO film of 700 Å thick, is settled down on a 3 mm thick Teflon pad. The Teflon pad together with a sapphire plate is put on a BK-7 plate with dimensions of $40 \times 5 \times 50$ mm.

The visualization from the side of heater surface is repeated stepwise. The test liquid, conditions and method are the same as those of experiment 1. In this case, the temperature of the ITO film is obtained from its relationship between temperatures and resistances.

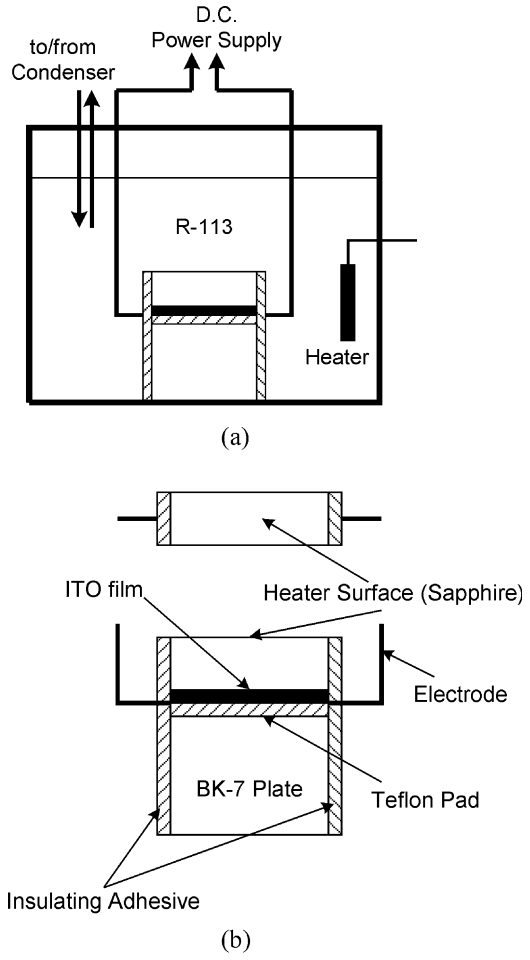

Fig. 3. Schematic diagram of the test apparatus to observe the side views of bubble structures: (a) experimental apparatus and (b) boiling surface.

And, the heater surface temperature is calculated from a steady state conduction equation.

2.3. Confirmatory test

The primary objectives of the confirmatory test are first to examine the pertinence of the simultaneous visualization of bubbles and dry areas, second to evaluate the degree of distortion from image processing.

The bottom part of a glass sphere simulating a bubble was cut to represent a dry spot, and machined to settle down on the heater. The holes resulting from the cut down simulate the different size of dry spots. Diameters of the simulated bubbles were measured carefully before experiments. The confirmation test was performed under non-heating condition by using the same method described in Section 2.1.

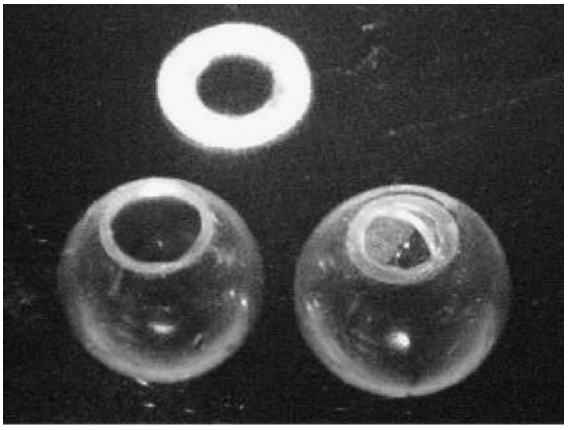

(a)

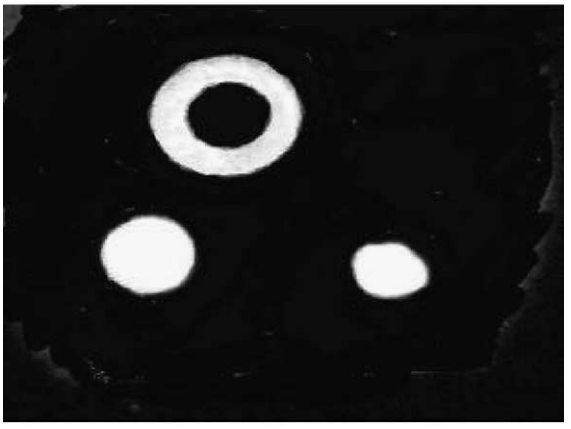

(b)

Fig. 4. Confirmatory test results: simultaneous visualization of (a) bubbles and (b) dry spots.

Fig. 4 shows the simultaneous visualization results for the bubbles and dry spots. In this figure, the dry spots are clearly shown. Also, the bubbles viewed from direct observation have complete spherical shapes, even though the optical path for direct reflection has limited observation angle. From the image processing, it is noted that the diameters of the bubbles and dry spots have approximately 3% and 4% distortion, respectively, compared to the real size of them. From the confirmatory test, we can conclude that the present optical method to simultaneously measure the bubble and dry spot sizes is very appropriate.

3. Experimental results

3.1. Visualization results

3.1.1. Chronological behavior of bubbles and dry spots

Fig. 5 shows the chronological sequence of bubbles and dry spots at the inception of boiling ($\Delta T_{ws} = 21.4$ K). Figs. 5(a) and (b) show bubble nucleation and growth. Fig. 5(c) and (d) are the situation at the moment before detaching, and finally the bubble disappears in the picture as shown in Fig. 5(e). The lower part of Fig. 5 shows the dynamic behavior of dry spots under the corresponding bubbles. When a bubble nucleates, a dry spot below it appears and exists while the bubble is growing. Finally, if the bubble is detached, the dry spot disappears instantaneously. The area of the dry spot is smaller than that of the projected area of the bubble. The total number of dry spots is equal to that of bubbles before the coalescence of bubbles takes place. From the present synchronized observation for the chronological behavior of bubbles and dry spots, it is noted that the dry spots and bubbles exist simultaneously. This means

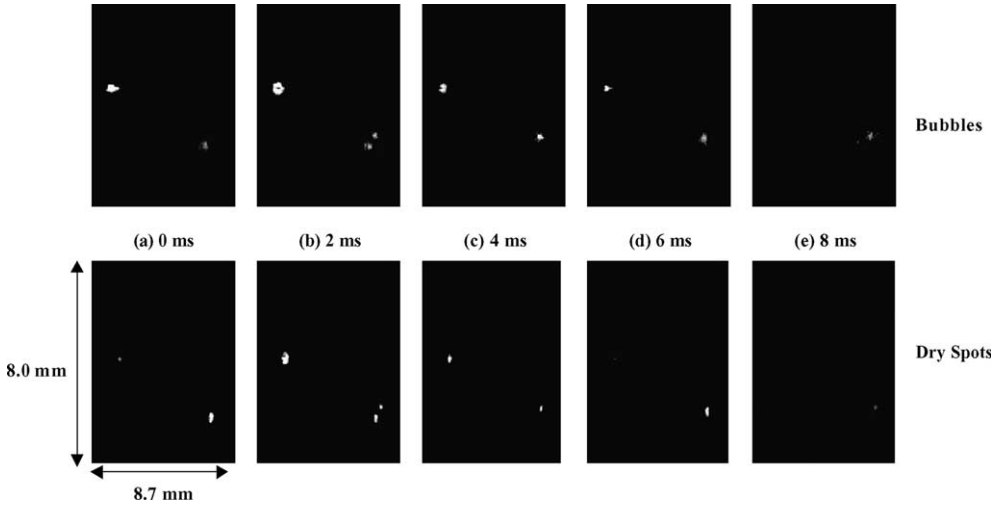

Fig. 5. Chronological dynamic behavior of bubbles and dry spots at incipience of boiling ($\Delta T_{WS} = 21.4$ K, $q = 25.9$ kW/m^2).

that when a bubble grows at a nucleation site, a dry spot is formed under the corresponding bubble.

3.1.2. Boiling regimes

Figs. 6 and 7 show a typical set of observed boiling phenomena from incipience of boiling to CHF. The pictures in Fig. 6 are the results of the synchronized observation and in Fig. 7 are the side views of bubbles. The identification indices in Figs. 6 and 7 correspond to regimes in the boiling curve given in Fig. 8.

3.1.2.1. Discrete bubble regime. Fig. 6(a) is a situation at incipience of boiling, and Fig. 6(b) and (c) shows the behavior of bubbles and dry spots at the discrete bubble region ($\Delta T_{ws} = 23.9$ and 29.5 K, respectively). Compared to the situation at incipience of boiling, many round-shaped discrete bubbles and dry spots are observed. At the early portion of the discrete bubble regimes, shown in Fig. 7(a) and (b), the interaction between bubbles does not distort the shape of them. Fig. 7(c) shows that their interaction at some higher heat fluxes retards the departure of bubbles and their shape is slightly distorted, but a discrete bubble regime is maintained. In this discrete bubble regime, the distinct feature is that the active site density is exactly the same as the dry spot density. The discrete bubble regime continues up to approximately 70% of CHF.

3.1.2.2. Coalesced bubble regime. At heat fluxes above 70% of CHF, the interaction between bubbles occurs actively. Fig. 6(d) represents the situation at approximately heat fluxes of 80% of CHF ($\Delta T_{ws} = 34.1$ K, $q = 112.1$ kW/m^2). Due to the lateral interaction between bubbles, some coalesced dry areas are observed to be larger than that of an isolated dry spot. The interaction process is clearly seen in Fig. 7(d). Even though some large dry areas are observed on the heater surface, the slope of boiling curves does not change apparently as shown in Fig. 8. From the video image analysis, the time-averaged resident time of large dry areas for the coalesced bubble regime is within 4 ms for the present study. Therefore, it is considered that the surface temperature does not increase during the short period of the large dry area.

3.1.2.3. Local vapor film regime ($\Delta T_{ws} = 38.0$ K, $q = 121.2$ kW/m^2). As the heat flux is increased above 80% of CHF, the bubble behaviors are somewhat different from those of the preceding heat flux cases as shown in Figs. 6(e) and 7(e). Most bubbles are coalesced with each other, and their shapes seem like vapor patches. As a result, the intensive interaction between dry areas occurs. Bubble behaviors observed from side window are illustrated sequentially in Fig. 9. Under a large departing vapor mass, a filmwise vapor bubble formed from the lateral coalescence of bubbles exists locally. The occurrence of the local filmwise vapor bubble results in the formation of an even larger dry area. And, the resident time of the large dry area under the filmwise vapor bubble is further increased comparing to those of the preceding heat flux regimes. This increased resident time of the large dry area influences the heat transfer mechanism and, consequently, the slope of the boiling curve becomes mild as marked (e) in Fig. 8. In the local vapor film regime, the liquid–wall contact fraction decreases below approximately 50% as shown in Fig. 11, and the wetting between dry areas shows a complex maze-like pattern as shown in Fig. 6(e).

3.1.2.4. Critical heat flux ($\Delta T_{ws} = 43.0$ K, $q = 139.9$ kW/m^2). In the present study, the CHF was defined as the highest heat flux that the heater surface temperature was kept stable before temperature excursion was commenced by a slight increase in heat flux. Fig. 10 shows

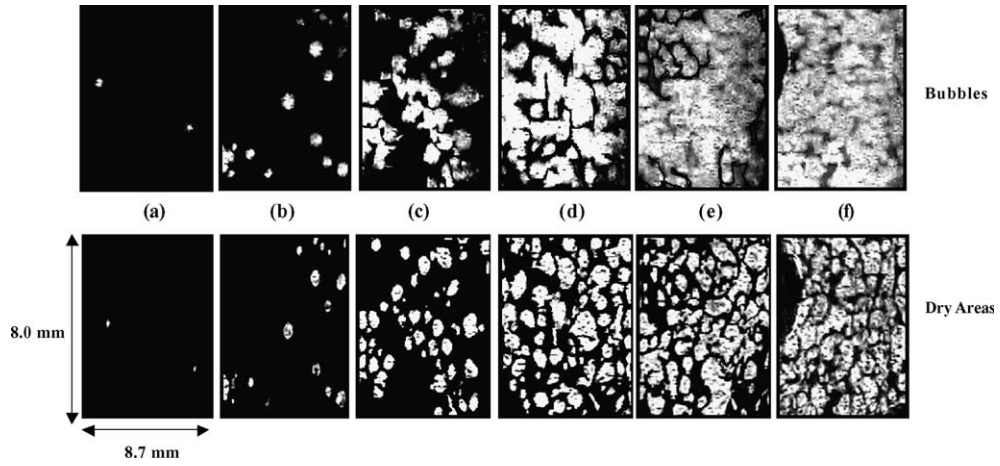

Fig. 6. Variations of bubbles and dry areas from incipience of boiling to CHF.

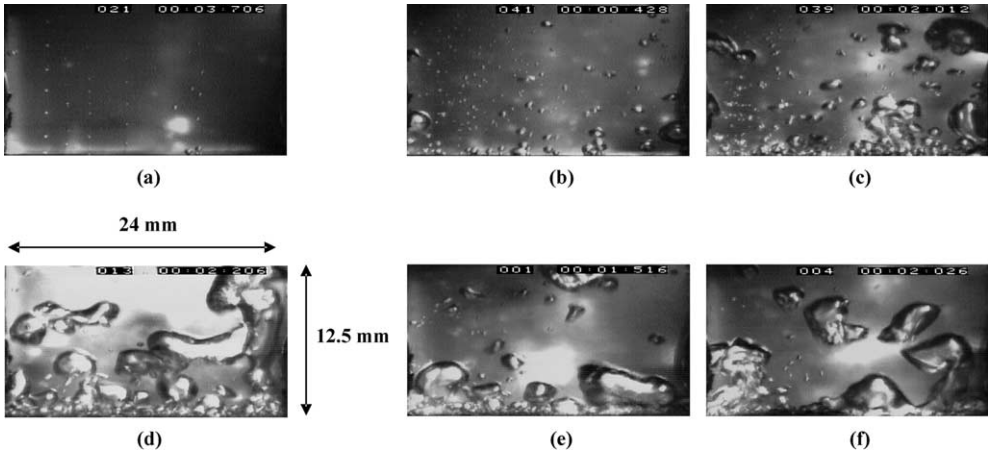

Fig. 7. Side views of bubble structures at each step of heat flux: (a) incipience of boiling, (b) discrete bubble regime, (c) discrete bubble regime, (d) coalesced bubble regime, (e) local vapor film regime and (f) CHF.

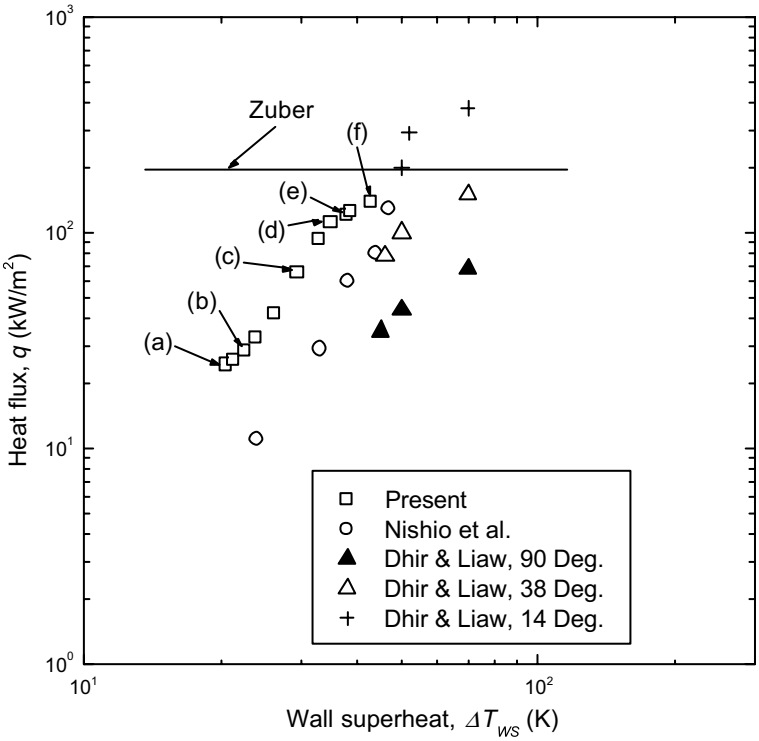

Fig. 8. Boiling curve for the present study with another predicted and measured ones.

the chronological dynamic behavior of bubbles and dry areas at CHF. As shown in Fig. 10, most of the heater surface becomes dry and the liquid–solid contact fraction decreases below 30% as shown in Fig. 11. In this situation the dry areas behave very violently with enlarging and shrinking. As a result, considerable interaction between dry areas occurs. During the violent behavior of dry areas, the wetted pattern is not a continuous plane type but maze-like curves. This wetted pattern is similar to the network pattern observed by Oka et al. [12] and Nishio et al. [7]. At the same time, the vigorous boiling occurs in wetted regions.

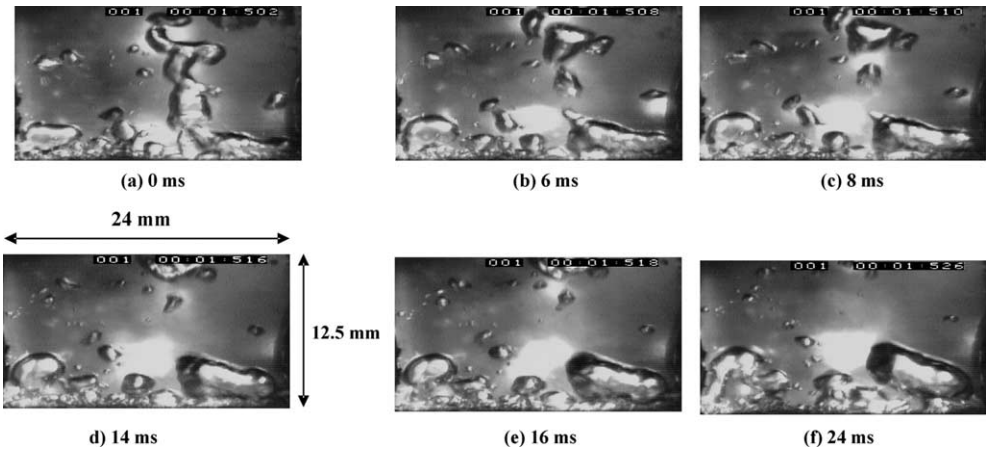

Fig. 9. Side views of bubble structures at local vapor film regimes ($q = 0.9q_{CHF}$).

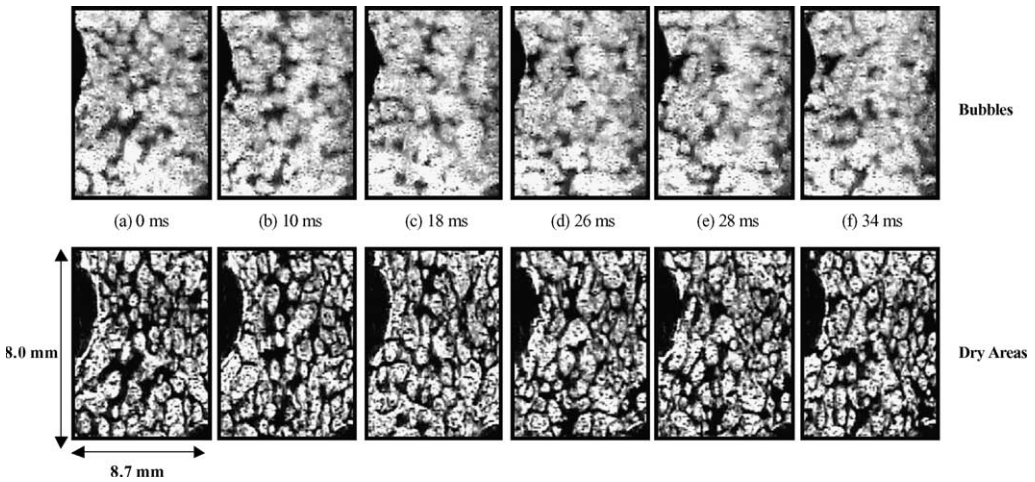

Fig. 10. Chronological dynamic behavior of bubbles and dry areas at CHF ($\Delta T_{WS} = 43.0$ K, $q = 139.9$ kW/m^2).

Due to a much smaller density ratio between liquid and vapor phase (ρ_f/ρ_g), the present liquid, R-113, gives a much greater vapor density than water at the same atmospheric pressure. The bubble mass flux in the water boiling test is expected to be much higher than the Freon boiling test. Therefore, we need to further investigate this effect on CHF using water or the liquid close to the density ratio of the water.

The side views of bubble structures at CHF are shown in Fig. 12. Even though the present test liquid is a well-wetting fluid, a large vapor film covers a great part of the heater surface. This experimental observation is similar to the observation on R-113 boiling by Nishio et al. [7], water boiling by Zhao et al. [14]. The vapor stems and the dryout of macrolayer have not been observed. Instead of the vapor stems and dryout of the macrolayer in the macrolayer dryout model by Haramura and Katto [2], the local nucleate boiling occurs under the large vapor film and at the edge of it. Experimental observation from the present study and other investigators [7,13,14] support the periodical existence of the individual bubble, local nucleate boiling, instead of the stationary vapor stems at CHF. Especially, intense nucleate boiling takes place around the edge of the vapor film. It is considered that this strip shape local boiling region around the edge of a large vapor film is equivalent to the wetted region in Fig. 10. From the video image analysis, the widths of the local boiling region in Figs. 10 and 12 are nearly equal as approximately 2.0 mm. Some nucleating bubbles in a locally wetted region coalesce laterally each other and form another small vapor film. This small vapor film does not grow large, and a wetting region is formed repeatedly. This type of local nucleate boiling is similar to the observation by Galloway and Mudawar [13] for flow boiling of FC-87.

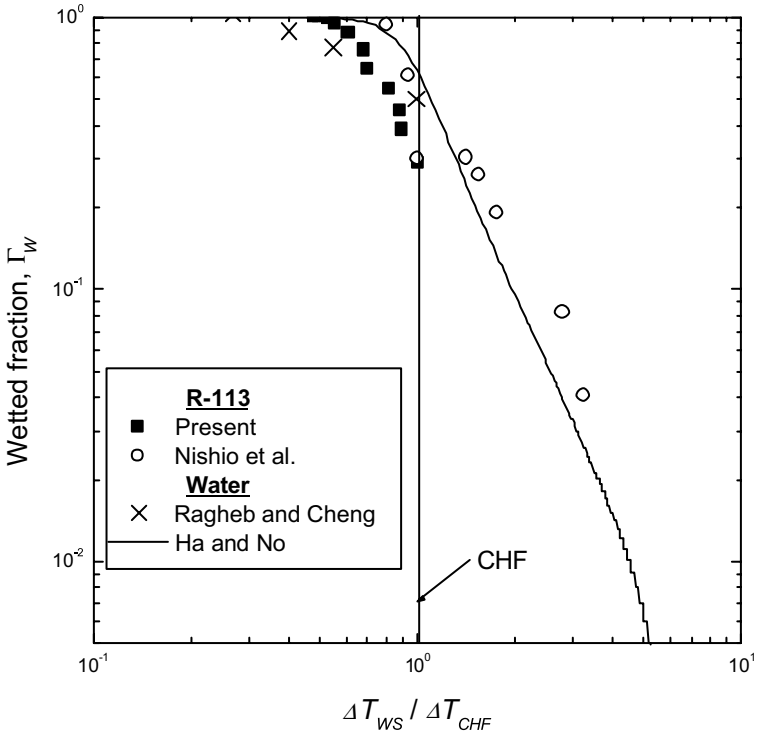

Fig. 11. Wetted fraction as a function of the surface superheat.

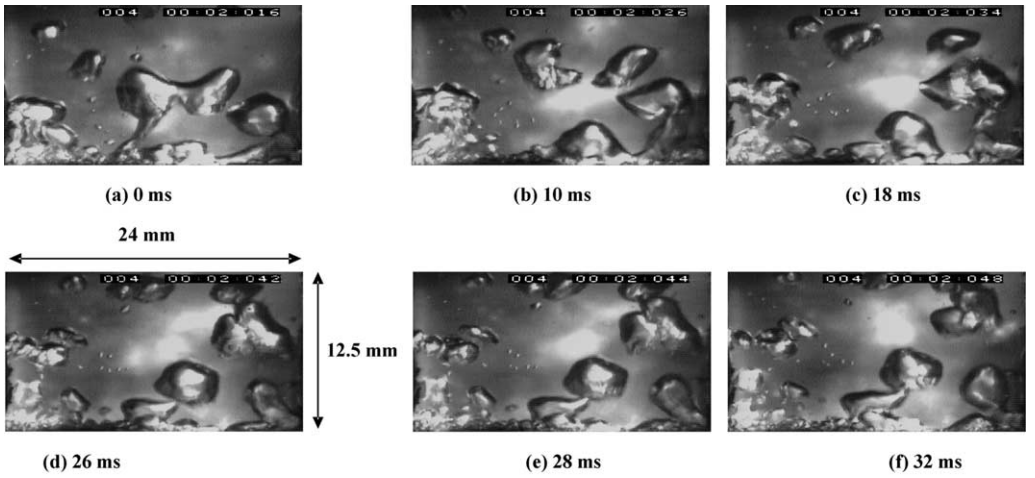

Fig. 12. Side views of dynamic behavior of bubbles at CHF.

A large vapor film, which covers a great part of the heater surface, collapses when its upper interface departs. After the large vapor film collapses, a short wetting occurs as shown in Fig. 12(c). If the surface is intermittently wetted, vigorous boiling occurs and a continuous vapor film resulting from the coalescence of vapor bubbles is reestablished as shown in Fig. 12(e). This phenomenon is similar to the observation by Nishio et al. [7]. From the above photographic analysis, it is noted that nucleate boiling takes place around the edge of the large vapor film and underneath the departing large vapor mass. This means that, even though the vapor film covers a large fraction of the heater surface, the local nucleate boiling in the wetted region plays a key role in determining the heater surface temperature not increasing it further.

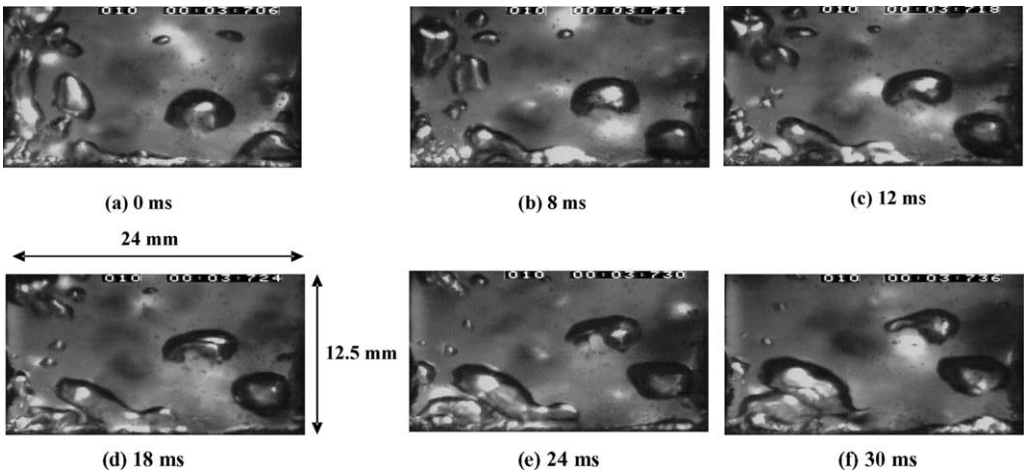

Fig. 13. Side views of dynamic behavior of bubbles just after CHF ($q = 1.06q_{CHF}$).

3.1.2.5. CHF triggering mechanism. At CHF, the slight increase of heat flux causes a commencement of temperature excursion. This situation just after CHF is defined as CHF(+). Photographs for CHF(+) are shown in Fig. 13. Even though the wavy motion of the large vapor film occurs actively, the liquid does not touch the heater surface, resulting in no wetting. Also, the formation of the wetted region due to the departure of a large vapor film, which is repeatedly seen at CHF, is not observed as in the case of CHF(+), while brief nucleate boiling occurs at the edge of a vapor film as illustrated in Fig. 13(a)–(c). However, the wetted region quickly becomes the dry region with a continuous vapor film and then nucleate boiling is limited as shown in Fig. 13(d).

From comparing the side views of bubble behaviors, some distinct differences in wetting modes between CHF and CHF(+) can be drawn. As described, at CHF, liquids were intermittently supplied to the surface through the repeated formation and collapse of the relatively small vapor film at the edge of the large one. Unlike CHF situation, there is little liquid penetration during the departure of a large vapor mass at CHF(+). Brief nucleate boiling is observed only at the wetted region near the edge of the vapor film as shown in Fig. 13(a)–(c). However, this brief wetting is extinguished by an agglomeration of nucleating bubbles as in Fig. 13(d). As a result of this limited nucleating boiling activity at the local wetted part of the heater surface, the heater surface temperature begins to increase further. Consequently, even though the surface temperature is well below the Leidenfrost temperature, the rewetting is precluded due to the agglomeration of nucleating bubbles at the local wetted region. These observations are similar to the reduced boiling activity by Galloway and Mudawar [13] and Celata et al. [15]. Once the continuous vapor film covers the whole heater surface, no nucleate boiling appears on the heater surface and the surface temperature begins to rise slowly from a stable value of approximately 90 °C. However, once the surface temperature exceeds approximately 108 °C, it begins to rise uncontrollably at a very faster rate. Finally burnout occurred. As discussed above, CHF(+) comes from the locally limited nucleate boiling activity rather than any changes of hydrodynamic conditions [16].

Comparing the present CHF mechanism to the dry spot model proposed by Ha and No [8], the dry spot model nearly incorporates the present observation. They postulated that when nucleating bubbles in a cell exceed critical number, the liquid supply into the cell stopped and dry spots occurred. Then, the dry spots coalesced with each other and CHF occurred. However, the dry spot formation mechanism is somewhat different from the present observation. Therefore, the dry spot model need to be modified to reflect the real dry spot formation mechanism.

The current CHF models are mainly based on the postulation on the CHF phenomena without physical observation. The new CHF models need to be consistent with the direct observation on CHF. Also, as several investigators suggested [8,11], a realistic CHF model would be one that gives a natural outcome for the description of the high-heat flux nucleate boiling region in contrast to the traditional view of CHF as independent phenomena distinct from the nucleate boiling. As discussed above, the present CHF mechanism, the locally limited nucleate boiling activity, gives us the possibility to model the CHF as the extension of the high-heat flux nucleate boiling.

3.2. Wall temperature measurement

As mentioned earlier, the heater wall temperatures were measured by two K-type thermocouples. Fig. 14

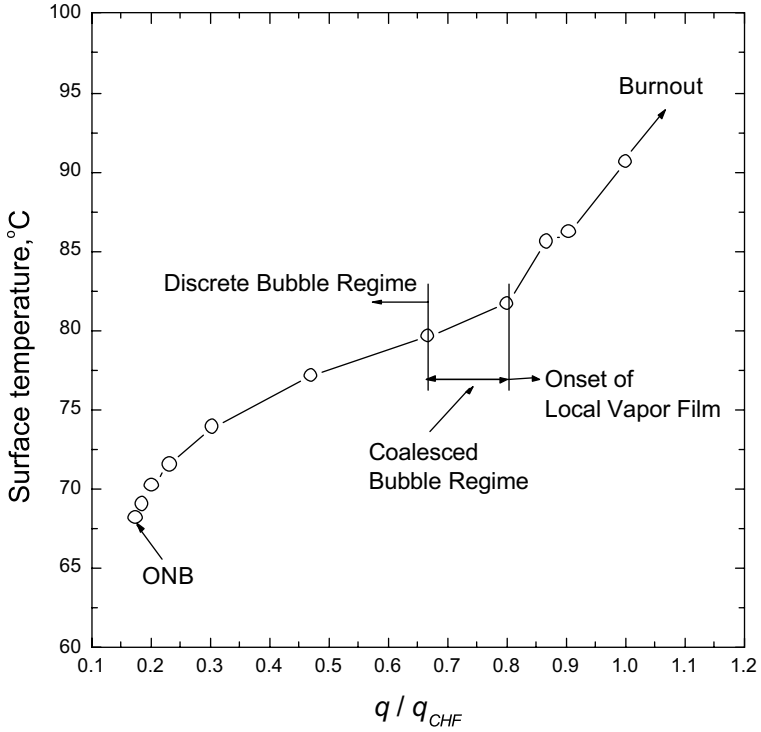

Fig. 14. Measured heater surface temperature as a function of the heat flux.

shows the time- and space-averaged surface temperature as a function of the heat flux along with the corresponding boiling subregime boundaries. In the early portion of the nucleate boiling region, the wall temperature curve is almost linear. As soon as the number of nucleating bubbles increases, the slope of the wall temperature curve apparently reduces and becomes flat. In this region, a large increase in the heat flux produces a small increase in the surface temperature. This enhanced heat transfer mode continues to the coalesced bubble regime. However, in the local vapor film regime, the slope of the temperature curve increases abruptly. This implies that the large dry area under the large vapor bubble contributes to the increase of the surface temperature. During the existence of the vapor film on the heater surface, the heat transfer between heater and liquid decreases due to thermal insulation. As heat flux is increased further, the stable filmwise bubbles cover the whole heater surface. Consequently, the nucleation of bubbles is limited and the surface temperature increases uncontrollably.

3.3. Active nucleation site density

As discussed at Section 3.1.2, the bubble density is exactly the same as the dry spot density in the discrete bubble regime. Therefore, it is reasonable to calculate the active site density considering the dry spot density. In this study, the active site density is counted only within the heat fluxes 80% of CHF. Above 80% of CHF, the counting of dry areas is impossible due to the intensive interaction. Fig. 15 shows the time-averaged active site density during 200 ms as a function of the surface superheat with another predicted ones [19,20]. The active site density increases drastically with the increase of wall superheat. However, the trend is nearly linear. The active site density is in the order of 10^5 in the fully-developed nucleate boiling region, and this result is nearly the same as that in the case of 18° by Wang and Dhir [19].

4. Conclusions

In the present study new experimental attempts are made to directly observe the physical boiling phenomena of bubbles and dry areas simultaneously from the bottom of the heater surface. In addition, we take the side views of bubbles to obtain the two-dimensional bubble behavior. From synchronized high-speed video imaging of bubbles and dry spots and the side views of bubble behaviors, the following conclusions can be derived:

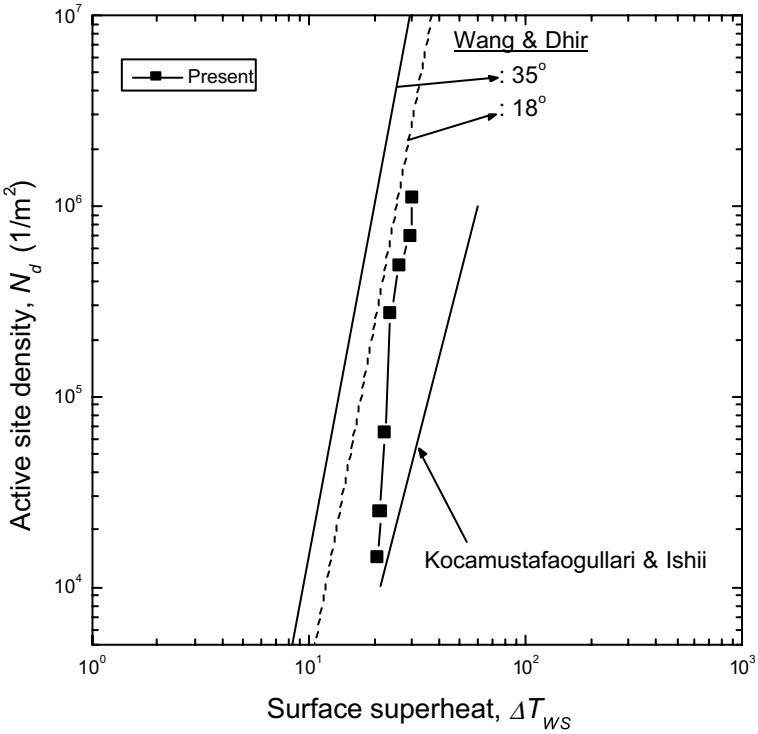

Fig. 15. Active nucleation site density as a function of the surface superheat.

(1) The formation of bubbles and dry spots occurs simultaneously. This indicates that when a bubble nucleates and grows at a nucleation site, a dry spot is formed under the corresponding bubble. Therefore, they should be considered as a synchronized identity rather than an independent one.
(2) The dry spot density is equal to the active site density up to the region of 70% of CHF heat flux.
(3) At CHF, the fraction of the dried area of the heater surface is above 70%. Also, the heater surface temperature is stably maintained due to the local nucleate boiling in the strip-shape wetted region existing around the edge of the vapor film. This implies that the heat generated in the heater is sufficiently extracted by the nucleate boiling at the locally wetted region.
(4) At CHF(+), the nucleate boiling region still exists but the rewetting region is extinguished by an agglomeration of nucleating bubbles. Then, dry spots under the agglomerated bubble grow, eventually resulting in the dryout of all heater surface. This means that, as the heat extract rate from the wall by nucleate boiling becomes smaller than the energy production rate in the heaters, the heater surface temperature begins to increase.
(5) It can be concluded that CHF is strongly related to the locally limited nucleate boiling activity at the wetted region. This gives us the possibility to model the CHF as the extension of the nucleate boiling.
(6) We need to further investigate the density ratio (ρ_f/ρ_g) effect on CHF using water or the liquid close to the density ratio of the water.

Acknowledgements

This work was financially supported by the nuclear R&D program from the Ministry of Science and Technology of Korea.

References

[1] R.F. Gaertner, Photographic study of nucleate boiling on a horizontal surface, ASME J. Heat Transfer 87 (1965) 17–29.
[2] Y. Haramura, Y. Katto, A new hydrodynamic model of critical heat flux, applicable widely to both pool and forced convection boiling on submerged bodies in saturated liquids, Int. J. Heat Mass Transfer 26 (1983) 389–399.
[3] V.K. Dhir, S.P. Liaw, Framework for a unified model for nucleate and transition pool boiling, ASME J. Heat Transfer 111 (1989) 739–746.
[4] D.B. Kirby, J.W. Westwater, Bubble and vapor behavior on a heated horizontal plate during pool boiling near

burnout, Chem. Eng. Prog. Symp. Ser. 61 (57) (1965) 238–248.

[5] H.J. Van Ouwerkerk, Burnout in pool boiling the stability of boiling mechanisms, Int. J. Heat Mass Transfer 15 (1972) 25–34.

[6] R.D.M. Carvalho, A.E. Bergles, The pool nucleate boiling flow patterns of vertically oriented, small heaters boiling on one side, in: Proceedings of the 10th International Heat Transfer Conference, Brighton, UK, vol. 5, 1994, pp. 25–30.

[7] S. Nishio, T. Gotoh, N. Nagai, Observation of boiling structures in high heat-flux boiling, Int. J. Heat Mass Transfer 41 (1998) 3191–3201.

[8] S.J. Ha, H.C. No, A dry-spot model of critical heat flux in pool and forced convection boiling, Int. J. Heat Mass Transfer 41 (2) (1998) 303–311.

[9] S.J. Ha, H.C. No, A dry-spot model for transition boiling heat transfer in pool boiling, Int. J. Heat Mass Transfer 41 (1988) 3771–3779.

[10] S.J. Ha, H.C. No, A dry-spot model of critical heat flux applicable to both pool boiling and subcooled forced convection boiling, Int. J. Heat Mass Transfer 43 (2000) 241–250.

[11] P. Sadasivan et al., Perspective: Issues in CHF modeling—The need for new experiments, ASME J. Heat Transfer 117 (1995) 558–567.

[12] T. Oka et al., Pool boiling of *n*-pentane, CFC-113, and water under reduced gravity: parabolic flight experiments with a transparent heater, ASME J. Heat Transfer 117 (1995) 408–417.

[13] J.E. Galloway, I. Mudawar, CHF mechanism in flow boiling from a short heated wall. I: Examination of near-wall conditions with the aid of photomicrography and high-speed video imaging, Int. J. Heat Mass Transfer 30 (10) (1993) 2511–2526.

[14] Y.H. Zaho et al., Boiling bubble behavior and heat transfer characteristics on a horizontal Pt-wire within a narrow space, in: Proceedings of heat transfer seminar of JSME, Okinawa, Japan, 1994, pp. 238–241.

[15] G.P. Celata et al., Visual investigation of high heat flux burnout in subcooled flow boiling of water, in: Third International Conference on Multiphase Flow, ICMF'98, Lyon, France, 1998.

[16] N. Zuber, Stability of boiling heat transfer, ASME J. Heat Transfer 80 (1958) 711–720.

[19] C.H. Wang, V.K. Dhir, Effect of surface wettability on active nucleation site density during pool boiling of water on a vertical surface, ASME J. Heat Transfer 115 (1993) 659–669.

[20] G. Kocamustafaogullari, M. Ishii, Interfacial area and nucleation site density during pool boiling of water on a vertical surface, Int. J. Heat Mass Transfer 26 (9) (1983) 1377–1387.

[21] ANSI/ASME PTC 19.1, ASME Performance Test Codes: Supplement on Instruments and Apparatus, Part 1: Measurement Uncertainty, 1985.